# Contact creep compliance of viscoelastic materials via nanoindentation

Catherine A. Tweedie and Krystyn J. Van Vliet[a)]
*Department of Materials Science and Engineering, Massachusetts Institute of Technology, Cambridge, Massachusetts 02139*

(Received 5 August 2005; accepted 22 March 2006)

The creep compliance of viscoelastic materials such as synthetic polymers is an established metric of the rate at which strain increases for a constant applied stress and can, in principle, be implemented at the nanoscale to compare quantitatively bulk or thin film polymers of different structures or processing histories. Here, we outline the evolution of contact creep compliance analysis and application for both conical and spherical indenter geometries. Through systematic experiments on four amorphous (glassy) polymers, two semi-crystalline polymers and two epoxies, we show that assumptions of linear viscoelasticity are not maintained for any of these polymers when creep compliance is measured via conical indentation at the nanoscale, regardless of the rate of stress application (step or ramp). Further, we show that these assumptions can be maintained to evaluate the contact creep compliance $J_c(t)$ of these bulk polymers, regardless of the rate of stress application, provided that the contact strains are reduced sufficiently through spherical indentation. Finally, we consider the structural and physical properties of these polymers in relation to $J_c(t)$, and demonstrate that $J_c(t)$ correlates positively with molecular weight between entanglements or crosslinks of bulk, glassy polymers.

## I. INTRODUCTION

Devices composed of small volumes of time-dependent materials, such as polymeric thin films, hydrated biological scaffolds, and microelectronic packaging, require mechanical characterization not attainable through well-developed methods suitable for bulk materials. Several categories of nanomechanical testing exist, including quasistatic nanoindentation,[1] dynamic nanoindentation,[2,3] nanomechanical contact creep,[4–10] and impulse indentation.[11] However, few analytical methods to interpret time-dependent material responses have been proposed that do not assume the material to be well-described as a linear viscoelastic solid. Despite frequent application of this assumption, this idealized response is not maintained in most nanomechanical experimental conditions on polymers, and this assumption can thus propagate quantitative and qualitative errors in analysis of polymer deformation. Time-dependent materials will behave as linear viscoelastic solids below a material-dependent, limiting elastic strain on the order of 1–2%. Stress, and thus strain, imposed on the material under contact loading such as nanoindentation may be reduced by decreasing the magnitude of the applied force $P$ or by increasing the area over which $P$ acts on the material. However, most instrumented nanoindenters have a fixed load range over which data can be acquired accurately, such that the indenter geometry and corresponding shape function are important experimental factors.

Nanomechanical creep testing has significant potential for interpreting the mechanical responses of polymers because the material response inherently includes time-dependent deformation. The shear creep compliance $J(t)$ is strictly defined as the change in strain as a function of time under instantaneous application of a constant stress, or

$$J(t) = \frac{\epsilon(t)}{\sigma_o} \quad , \tag{1}$$

and provides a means to quantify the capacity of a material to flow in response to a sudden applied stress.[12] Although conventional measurements of $J(t)$ included uniaxial or simple shear stress, researchers have increasingly reported creep compliance interpretations of instrumented (conical and spherical) indentation experiments on bulk or thin film polymers. However, due to the nonlinearities in material behavior and contact mechanics, current experimental investigations of creep compliance

[a)]Address all correspondence to this author.
e-mail: krystyn@mit.edu
DOI: 10.1557/JMR.2006.0197

 

typically assume particular linear viscoelastic models to fit the creep response. Figure 1 schematically illustrates the linear viscoelastic creep response at various applied stresses. The doubling of the instantaneous and constant applied stress $\sigma_1$ exactly doubles the strain $\epsilon(t)$ for any time $t$ during creep [Fig. 1(a)]. It is well-established that the creep compliance $J(t)$ for a linear viscoelastic material is invariant with applied stress [Fig. 1(b)] due to the linear relationship between stress and strain at any time point for such materials. Referencing Eq. (1), a polymer for which $J(t)$ changes as a function of maximum instantaneous stress $\sigma$ does not conform to the assumptions of linear viscoelasticity. That is, $J(t)/\sigma(t) \neq k$ where k is a constant, due to the nonlinear constitutive relations of that particular polymer and/or to induced strain in excess of the linear viscoelastic strain limit for that material. In either case, polymers that do not exhibit $J(t)/\sigma(t) = k$ for a given indenter geometry and load/stress range cannot be characterized accurately by models that implicitly assume a purely linear viscoelastic response. Further, the models from which most expressions for creep compliance $J(t)$ expressions are derived were developed to determine the pressure distribution for axisymmetric indenter contact on viscoelastic solids[12,13] and simplified for the case of step loading. In actuality, few nanomechanical instruments can attain the step-load condition because of limitations in speed of data acquisition and in force resolution. Thus, "quasi-step" loading, where the minimum loading time documented thus far for the step-load experiment is 1 s,[5,6,14] is often used. Loading rate has been demonstrated to have an effect on the creep response,[5,9] and corrections for ramp loading have been proposed for a specific linear viscoelastic constitutive relation.[10]

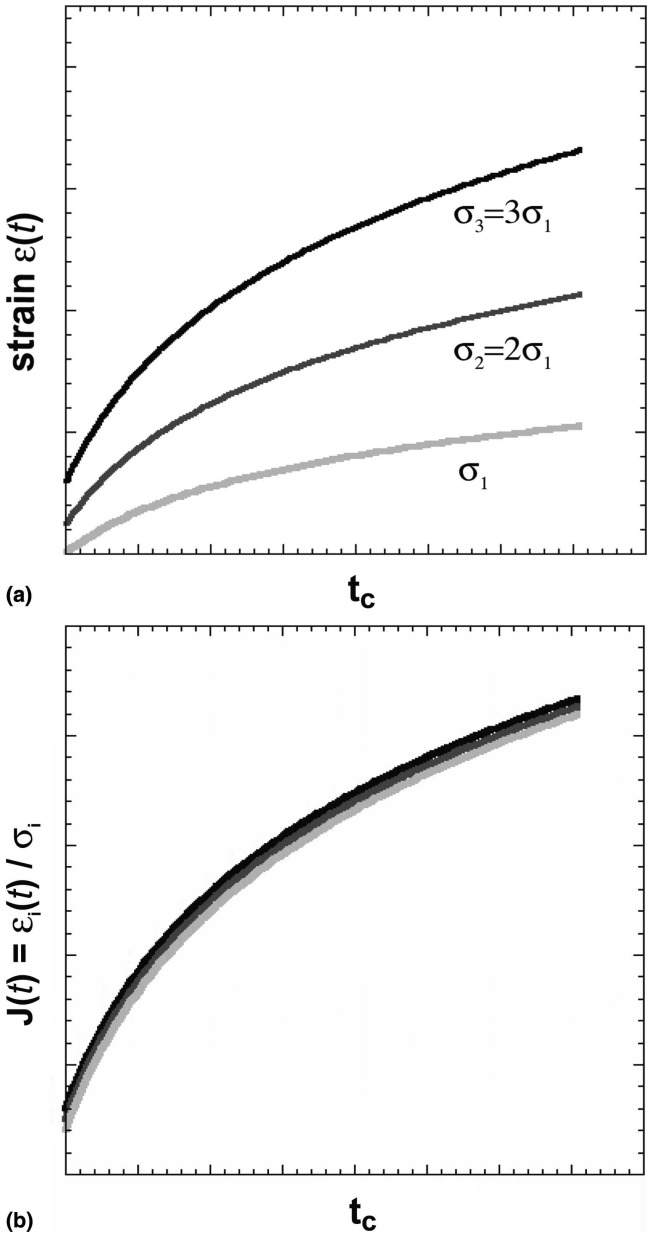


FIG. 1. (a) Ideal linear viscoelastic behavior is illustrated as strain $\varepsilon$ as a function of time during creep $t_c$ for three instantaneous and constant levels of applied stress $\sigma_i$. (b) Creep compliance $J(t)$ for a linear viscoelastic material is characteristic of that material and independent of $\sigma_i$.

In attempts to attain the linear viscoelastic deformation regime during indentation-enabled creep, several studies have included rounded conical probes ($R$ = 10 and 20 μm,[6,14,15]) and spherical probes ($R$ = 3.4 μm[5] to 150 μm[10]). However, it is not generally considered or demonstrated whether polymers conform to the idealized linear viscoelastic response of Fig. 1(b) under the contact creep conditions used, with notable exceptions.[7,10] Often, $J_c(t)$ is evaluated among polymers for only a single $P_{max}$,[9,14] such that load dependence cannot be ruled out. Lu et al. posited that, because indentations below a critical indentation depth (unique to each of two amorphous polymers considered) were not observable post-indentation via scanning electron microscopy, recovery implied linear viscoelasticity.[5] However, such indentation recovery does not ensure a linear path in either loading or unloading; linear viscoelastic deformation of these materials under indentation was neither proved nor disproved. Recent approaches to determination of $J_c(t)$ or linear viscoelastic operators based on the contact creep response are summarized in Sec. II. C, including those that also consider the limits of a linear viscoelastic creep response. As $J_c(t)$ is often interpreted within the framework of phenomenological models of linear viscoelastic behavior, for which there can be several distinct forms that reasonably fit a measured contact creep response, it is useful to also consider how $J_c(t)$ can be related to the structure and physical properties of polymers.

The contact creep compliance $J_c(t)$ is calculated herein primarily to demonstrate when the implicit assumption of linear viscoelastic deformation is obtained experimentally

and to consider how the material response changes with both polymer/monomer structure and loading conditions. Creep compliance formulations for conical and spherical indenter geometries are outlined and compared, and recent extensions are discussed. The contact creep compliance of eight bulk (semicrystalline and amorphous) polymers is then characterized with a Berkovich indenter that can be approximated as a conical geometry; none of the polymers behave as linear viscoelastic materials under these conditions. In contrast, the creep compliance of a subset of these same polymers under the same creep loads exhibits linear viscoelastic behavior for a spherical indenter of $R = 500\ \mu m$. These results illustrate the limit of linear viscoelastic analyses in nanomechanical creep compliance characterization and also demonstrate the relative effects of monomer structure, molecular steric hindrance, and microstructure on the contact creep compliance of bulk polymers.

## II. BASIS AND IMPLEMENTATION OF CONTACT CREEP COMPLIANCE SOLUTIONS

As demonstrated below, although the conditions required for accurate creep compliance determination according to Eq. (1) are typically not maintained in indentation-enabled creep experiments, this characterization of time-dependent flow can be used to compare materials and/or consider the microstructural determinants of polymer deformation. For this reason, we delineate creep measured via instrumented indentation as contact creep compliance $J_c(t)$, underscoring the fact that load and not stress is maintained constant in such experiments. The majority of viscoelastic solutions used to interpret contact creep compliance derive from two independently obtained derivations to the general problem of contact between a rigid symmetric body and a viscoelastic halfspace. These solutions for creep compliance in shear $J(t)$, reported by Lee and Radok (1960) and by Ting (1966), were elegant responses to an analytical challenge: viscoelastic deformation for which the Laplace transform could not be readily applied to predict stress distributions under contact loading (see Appendix A). Here, we state the relevant solutions of Lee and Radok (LR-) and Ting (T-), and summarize recent implementation in experimental investigations of creep for bulk and thin film polymers.

### A. Solutions for spherical indenter geometry

The LR-solution for creep compliance in shear under spherical indentation where $a \ll R$ under a constant applied load $P_o$ can be stated as

$$J_c(t) = (1 - \nu)J(t) = \frac{8\sqrt{R}}{3P_o}\left[h(t)\right]^{3/2}] \quad , \tag{2}$$

whereas the T-solution for the same condition can be stated as

$$\phi(t) = \frac{8\sqrt{R}}{3P_o}\left[h(t)\right]^{3/2}] \quad , \tag{3}$$

such that $\phi(t) = (1 - \nu)J(t)$ for constant $\nu$, or $\phi(t) = 1/2J(t)$ for incompressible materials for which $\nu = 1/2$. Ting states that $\phi(t)$ is of the general form of creep compliance but does not explicitly equate $\phi(t)$ to $J_c(t)$. Neither solution of the pressure distribution actually requires step-loading of the viscoelastic material, but both solutions are simplified by this constraint and implicit in the representations of $J_c(t)$ for Eqs. (2) and (3).

### B. Solutions for conical indenter geometry

Lee and Radok did not consider conical indenter geometries, presumably due to the constraint of "small strains" imposed by linear viscoelastic operators. However, Ting presented a general solution for any smooth, axisymmetric indenter profile and provided specific solutions of total contact pressure for conical, spherical, and paraboloidal (classic sphere for $a \ll R$) geometries. The T-solution for $\phi(t) = 1/2J(t) = J_c(t)$ under an instantaneously applied and constant depth $h_o$ is generally given by Eq. (A11) of Appendix A. For a conical indenter of semi-apex angle $\alpha = \pi/2 - \theta$, where $\theta$ is the angle between the material free surface and inclined indenter surface assumed by Ting, contact creep compliance $J_c(t)$ is

$$J_c(t) = \frac{2\pi a^2(t = 0)\tan\theta}{P(t)} \quad . \tag{4}$$

For the case more accessible to instrumented indentation experiments, an instantaneously applied and constant force $P_o$,

$$J_c(t) = \frac{2\pi a^2(t)\tan\theta}{P_o} = \frac{8\tan(\alpha)h^2(t)}{\pi P_o} \quad . \tag{5}$$

As stated in Eq. (5), $J_c(t)$ can be calculated directly from experimentally measured $h(t)$ for a known indenter semi-apex angle $\alpha$. Although this calculation is straightforward and the average contact stress for a conical indenter is maintained constant by virtue of the self-similar geometry, the stress singularity at the cone apex immediately violates the assumption of linear (or small strain) viscoelastic deformation.

Equations (2)–(5) represent the principal relations for determining creep compliance from contact loading, i.e., indentation-enabled creep experiments. Equations (3) and (5) are used to analyze the experiments in the present study. These equations assume linear viscoelasticity but do not assume any particular form of the constitutive relation in terms of the nature of the linear viscoelastic

operators. More simply, these solutions do not presuppose configurations of springs and dashpot elements that describe phenomenologically the stress or strain of a real polymer at short and long times. However, both Lee and Radok[13] and Ting[12] illustrate an application for indentation of a Maxwell solid. Ting thus shows that a decrease in applied load need not result in a decrease in contact area for a conical indenter geometry—an analytical prediction of the so-called "nose effect" observed during indentation unloading of polymers under insufficiently rapid unloading rates.[16,17]

### C. Extensions and applications of $J_c(t)$ models

Here, we briefly outline the extensions and adaptations of these solutions by others who have subsequently determined $J_c(t)$ via indentation for specific polymers and loading conditions. First, we consider approaches that do not assume a particular form of the linear viscoelastic operators and compare polymer response directly on the basis of measured $J_c(t)$.[5,7] Next, we consider approaches that inherently assume a spring-dashpot constitutive response of the polymer (such as the standard linear solid model[6,9,10,14,18]) from which model-dependent constants can be obtained.[9,10,14] As discussed, it is possible to demonstrate whether the condition of linear viscoelastic deformation is met with either approach.

Lu et al. adapted the solutions of Sneddon,[19] Ting,[12] and Lee and Radok[13] to extract viscoelastic properties from contact creep experiments via spherical and conical indenter geometries.[5] The authors found less than 10% error of $J_c(t)$ calculated during quasi-step loading with conical or spherical indenters [for amorphous poly(methyl methacrylate) (PMMA) and polycarbonate (PC)], in contrast to $J(t)$ measured in separate experiments via conventional uniaxial (PMMA) or shear (PC) creep compliance measurements. However, the contact creep conditions were not demonstrated to be independent of creep load $P_o$. In contrast, Van Landingham et al.[7] have recently applied Ting's solution for a constant applied load $P_o$ to compute $J_c(t)$ for amorphous (glassy) polymers and epoxies under conical indentation-enabled creep experiments. The authors superposed a cyclic load during a dwelling period at each of several distinct $P_o$ to obtain the projected contact area $A_c(t)$ for each data point during the dwelling period rather than calculate $J_c(t)$ directly from $h(t)$ and found that none of the polymers analyzed via Berkovich conical indentation and Eq. (5) were well-described as linear viscoelastic: $J_c(t)$ was not independent of applied load.

Although $J_c(t)$ can be determined quantitatively without recourse to a particular linear viscoelastic constitutive relations via Eqs. (2)–(5), the experimentally observed $h(t)$ can also be fit to a particular form of the creep function. Yang et al.[9] did not consider the elastic or viscoelastic contact solutions rigorously but rather applied the constitutive relations for a Kelvin-type solid (a series of parallelized springs $E_i$ and and dashpots $\eta_i$ of established $\sigma$-$\varepsilon$ relations) to a flat punch to determine $h(t)$ and thus

$$J(t) = \frac{h(t)}{\sigma_o h_{in}} = \sum_i J_i \quad , \tag{6}$$

where $h_{in}$ is an empirically determined length scale, and the form of $J_i$ represents the number of Kelvin-type elements in series that exhibit the characteristic depth decay of $(1 - e^{t/\tau}{}_i)$. The authors considered several amorphous polymers but could not correlate known physical or monomer structure/properties with the creep compliance quantified in this way. In contrast, Cheng et al.[14] and Oyen[10] adapted the Lee and Radok-solution to interpret spherical indentation creep on the basis of a standard linear solid model (i.e., a spring in series with a Kelvin–Voigt parallel spring and dashpot), via the method of Laplace transforms[5,14] or direct solution of the viscoelastic integral equations.[10] Defining $J_c(t)$ in terms of a constitutive model enables tractable solutions of constants defined by the model, but it is well understood that the number and magnitude of linear operators (or Prony series constants) is not unique and that several such sets can accurately describe a measured creep response. The resulting constants or material properties extracted from these fits necessarily depend on both the material and the form of the constitutive model that defines the creep function. Within a given study assuming a specific model, results among polymers can be compared, but it is then difficult to compare among studies or interpret $J_c(t)$ as a function of the structure and physical properties of these polymers. Cheng et al. described $J_c(t)$ generally as

$$J_c(t) = \sum_{i=1}^{N} J_i e^{-t/\tau_i} \quad , \tag{7}$$

where constants were determined through fits to experimental data and represented rather involved algebraic functions of the simple linear solid constitutive relations from which element constants $E_1$, $E_2$, and $\eta$ could ultimately be determined. The authors found that the indentation elastic modulus $E_i$ agreed well with $E_1$ extracted from the creep-type experiments for amorphous polystyrene and semicrystalline polymer poly(vinyl alcohol) at very low relative humidity (10%) but disagreed significantly at higher relative humidity, attributing this discrepancy in part to increased viscoelasticity under higher humidity. Oyen tested the applicability of the standard linear solid model to several polymer films by fitting a different linear viscoelastic creep function for a spherical indenter geometry ($R = 150$ μm) under single-ramp and

multi-step ramp loading to extract associated time constants and instantaneous shear modulus $G$.[10] Successful prediction of $h(t)$ was demonstrated for an order of magnitude increase in loading time (20 to 200 s) and a factor of two increase in maximum load (50 to 100 mN), indicating that this linear viscoelastic material model could be applied to contact creep analysis under specific (loading and environmental) conditions. That is, rather than showing that measured $J_c(t)$ was independent of load, the author demonstrated additivity required of linear viscoelasticity: the creep function form accurately predicted the $h(t)$ response measured at multiple creep loads.[10]

In the present study, we sought to determine the experimental conditions under which the assumptions implicit in Eqs. (2)–(5) hold, such that $J_c(t)$ can be measured within the linear viscoelastic regime. Further, rather than fit $J_c(t)$ to a particular linear viscoelastic constitutive model, we considered $J_c(t)$ as it relates to the molecular structure and physical properties of a range of well-characterized bulk polymers.

## III. EXPERIMENTS

### A. Materials

Common engineering polymers with relatively simple monomer structures were chosen for these contact creep experiments. These materials included four injection-molded, amorphous polymers [PC, polystyrene (PS), and PMMA of two different weight-average molecular weights $M_w$, commercially named Lucite (LU) and Plexiglas (PL)], as well as two epoxies in which the effective structural length scale is the molecular weight between crosslinks $M_c$: E3 ($M_c$ = 380 g/mol) and E8 ($M_c$ = 818 g/mol) as reported by Lesser et al.[20] In such chemically crosslinked, amorphous polymers, molecular chain mobility, or the ability for a given macromolecular chain to displace with respect to the network, increases with increasing $M_c$.[21] In addition, two injection molded, semicrystalline polymers were considered [polyethylene (PE) of 69% crystallinity and polypropylene (PP) of 58% crystallinity, as determined by small-angle x-ray diffraction]. The monomer structure, glass transition temperature $T_g$, and $M_w$ for each polymer are listed in Table I. All polymers were stored and tested at ambient temperature and relative humidity ($T$ = 22.2 °C, RH < 55%). The $T_g$ of all polymers excluding epoxies was measured via differential scanning calorimetry (DSC) as reported by the manufacturer (DuPont, Wilmington, DE) and confirmed in the present study, while the $M_w$ was determined by the manufacturer via gel permeation chromatography (GPC).

### B. Instrumented indenter-enabled contact creep testing

Nanoindentation-enabled creep experiments were conducted on an instrumented nanoindenter (MicroMaterials, Ltd., Wrexham, UK) to obtain indenter displacement into each polymer surface as a function of maximum load $P_{max}$, loading rate d$P$/d$t$, and indenter geometry. Indenter geometries included a diamond Berkovich (trigonal pyramid) indenter of cone-equivalent semi-apex angle $\alpha$ = 71° and a ruby sphere of radius $R$ = 500 μm.

As-processed root-mean-square sample surface roughness was <20 nm for all samples, as measured via contact-mode scanning-probe microscopy (3DMFP, Asylum Research, Santa Barbara, CA). Samples were stored in dessicators before and after testing, and surfaces were not chemically or mechanically modified prior to experimentation. Polymers were aged 2 h prior to testing in an instrument chamber that maintains humidity at 55% relative humidity (RH).

Creep tests were conducted to several $P_{max}$ (1, 5, 10, and 15 mN) for each of two d$P$/d$t$ [ramp loading

TABLE I. Model polymer systems.

| Polymer name | Structural formula | $T_g$ (°C) | $M_w$ (g/mol) |
|---|---|---|---|
| Polyethylene<br>PE | 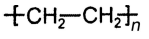 | −30 | 85,195 |
| Polypropylene<br>PP | 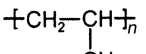 | 6 | 343,326 |
| Polystyrene<br>PS | 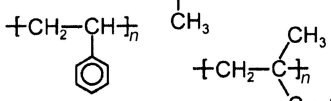 | 103 | 248,670 |
| Poly(methyl methacrylate) | | | |
| LU: Lucite[a] | 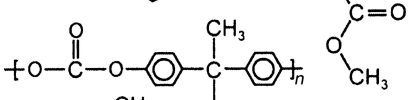 | 114 | 1,042,916 |
| PL: Plexiglas[b] | | 117 | 2,588,744 |
| Polycarbonate<br>PC | 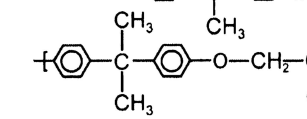 | 145 | 18,000 |
| Epoxy |  | … | $M_c$: |
| E3 | | | 380 |
| E8 | | | 818 |

[a]Rohm and Haas.
[b]Ineos Acrylics.

(0.5 mN/s) and rapid "quasi-step" loading (0.5 s to $P_{max}$)], as well as to $P_{max} = 30$ mN for ramp loading only. The quasi-step loading over a constant elapsed time required variation of loading rates to ensure sufficient data point acquisition at increased speeds (2, 10, 20, and 30 mN/s). For each pair ($P_{max}$, d$P$/d$t$), constant load $P_{max} = P_o$ was maintained for 10, 60, or 100 s to acquire $h(t)$. During this holding period approximating creep conditions, $P$ did not vary more than 2%; for "quasi-step" loads, the overshoot of the desired $P_o$ did not exceed 10% for the range of polymers considered. Indentation depths ranged between 300 and 2500 nm for experiments with the Berkovich indenter geometry and between 50 and 300 nm for the spherical indenter geometry. Typical drift in the displacement signal at room temperature is 0.01 nm/s. Each sample was tested at least in triplicate for each loading condition for the Berkovich indenter geometry. The two epoxy samples were tested in triplicate to all loading conditions with both the Berkovich and spherical indenter geometries. Equation (3) or (5), as appropriate for the indenter geometry used, was fit to the acquired $h(t)$ response, where $t_c$ is the elapsed time after attainment of the maximum contact load $P_o$ via step or ramp loading; that is, both step and ramp loading creep were evaluated from $h(t_c = 0)$.

## IV. RESULTS AND DISCUSSION

### A. Nanoindentation contact creep with a sharp indenter

#### 1. Nonlinear viscoelastic deformation

Eight common engineering polymers, with monomer structures and physical properties outlined in Table I, were evaluated at several distinct $P_{max}$ values with a Berkovich (sharp trigonal pyramid) indenter. The contact creep compliance, calculated using the model-independent formulation of $J_c(t)$ in Eq. (5), exhibited a positive dependence on increasing $P_{max}$ for all the polymers tested, confirming nonlinear viscoelastic behavior under these contact creep conditions for structurally simple amorphous polymers. Similar values for contact creep compliance of polymeric materials with a Berkovich indenter geometry were found in other recent studies.[9,15] Figure 2(a) shows the typical variation of $J_c(t)$ with $P_o$ ranging from 3 to 15 mN, and Fig. 2(b) compares all polymers for $P_o = 3$ and 15mN at $J_c(t = 10$ s). Note that in response to an increase in $P_{max}$ by a factor of five, all amorphous polymers exhibited a marked increase in $J_c(t)$ at the higher $P_{max}$, and therefore all amorphous polymers exhibited nonlinear viscoelastic deformation under these conditions. Although $J_c(t)$ can be calculated according to Eq. (5), the inherent assumptions of this calculation are not maintained. Therefore, the data are discussed in terms of monomer and microstructural

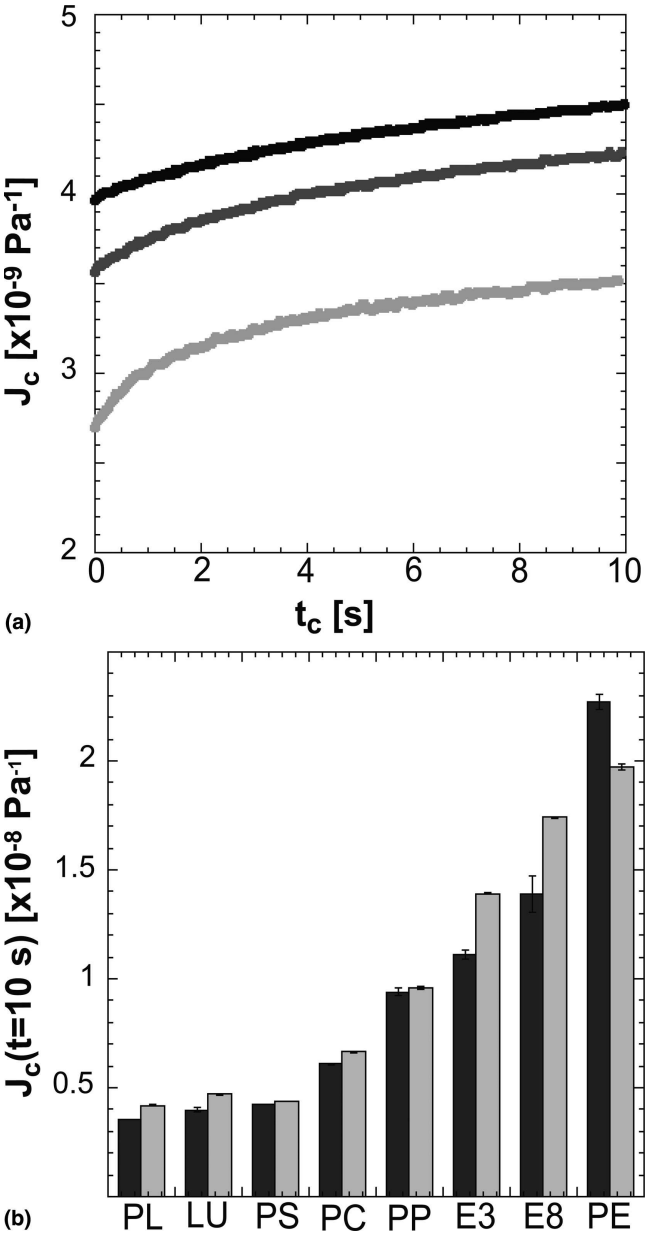


FIG. 2. Contact creep compliance $J_c(t)$ under ramp loading of 0.5 mN/s via Berkovich (sharp) probe. (a) PL shows typical dependence on creep load for $P_o$: 3 mN (light gray), 15 mN (dark gray) and 30 mN (black). (b) Comparison among all polymers at $J_c(t = 10s)$ for $P_o$: 3 mN (black) and 15 mN (gray) indicate increasing $J_c(t)$ with decreasing steric hindrance. Polymer abbreviations are as follows: PMMA PL, PMMA LU, PS, PC, PP, PE, and two epoxies, E3 and E8.

determinants of creep-like resistance to viscoelastoplastic flow in Sec. IV. C.

Plastic flow is a competing deformation mechanism under indentation-enabled creep compliance.[22,23] One way to assess the extent of plasticity is to subtract the creep portion of the displacement from the loading-unloading cycle and determine the extent to which the corrected, final depth of indentation $h'_f$ exceeds the maximum depth of indentation prior to the creep segment

$h_{max}$. The ratio $h'_f/h_{max}$ is proportional to the percent plastic work $W_p/W_{total}$.[24] We found that, for the Berkovich indenter geometry, $h'_f/h_{max}$ was as great as 62% in the amorphous polymers considered herein, indicating that there was indeed deformation that was not recovered during the unloading cycle of the indentation experiment. As we have shown via scanning probe microscopic examination of post-indentation recovery of Berkovich indentation in these same polymers,[25] although the depth of indentation does continue to recover over the next 48 h post-indentation, the volume of indentation does not recover appreciably because the material at the indenter sidewalls (where two facets of the pyramid join) remains plastically deformed over at least 48 h post-indentation.

### 2. Effect of loading rate d*P*/d*t*

Contact creep experiments conducted with a sharp conical indenter induce not only a load-dependent response but also a loading rate-dependent response. This point is illustrated in Fig. 3(a) where $J_c(t)$ of the low-$M_c$ epoxy E3 is shown for three maximum loads ($P_o$ = 1, 5, and 15 mN) for both ramp and step loading. The increase in loading rates induces an increase in $J_c(t)$ at all $P_o$ considered, as rapid loading to $P_o$ minimizes energy dissipation through viscous mechanisms, while slow loading to $P_o$ enables concurrent elastic and viscous responses prior to creep. Figure 3(b) demonstrates the effects of increased chain mobility on this loading rate dependence under conical indentation creep, comparing $J_c(t)$ for E3 (low $M_c$) and E8 (high $M_c$) for three $P_{max}$ attained via ramp loading (d$P$/d$t$ = 0.5 mN/s). As expected from Fig. 2(b), the increase in $M_c$ causes an increase in the $J_c(t)$ for all conditions. Surprisingly, the polymer of lower $M_c$, and thus lower molecular chain mobility, exhibits a greater dependence on load. This result is consistent with the pair of amorphous polymers PC (lower $M_w$) and PL (greater $M_w$), in which case the polymer with fewer entanglements and greater chain mobility (PC) is affected less by changes in load than the polymer with less chain mobility (PL) during contact creep. Experiments performed by Van Landingham et al.[15] demonstrated the same trend for PMMA and an epoxy: creep tests were carried out between $P_{max}$ = 0.2 and 10 mN on PMMA and epoxy samples (different from the epoxies detailed herein). Although the epoxy was slightly stiffer than the PMMA upon loading, $J_c(t)$ for the epoxy was more sensitive to changes in $P_{max}$. Together, these results indicate that contact creep compliance of polymers with lower chain mobility are more sensitive to changes in applied load. Here, for the Berkovich indenter geometry, an increase in $P_o$ by an order of magnitude resulted in a maximum increase in $J_c(t$ = 10 s) of 57% (E8 epoxy). However, we note that to support this effect of chain mobility on load dependence rigorously, complementary experiments are required to maintain a constant loading time for a range of loads $P_o$. More importantly, although trends with monomer rigidity, $M_w$, and $M_c$ are observed in $J_c(t)$ as measured via a sharp conical indenter geometry, the dependence of this response on applied load and loading rate indicate highly nonlinear behavior that is not interpreted accurately via standard linear viscoelastic analytical functions.

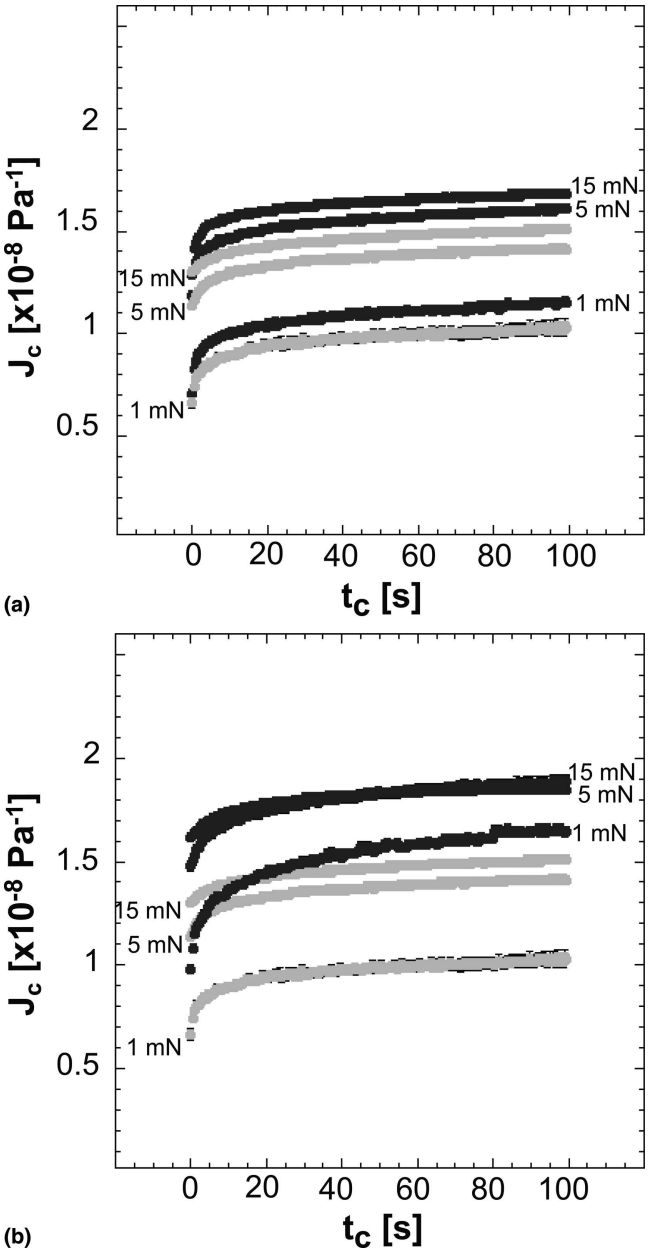


FIG. 3. (a) Comparison of creep compliance $J_c(t)$ for step (black) and ramp (gray) loading for a single epoxy (E3) indented with a Berkovich indenter at three maximum loads: 1 mN, 5 mN and 15 mN. (b) Comparison of $J_c(t)$ for two epoxies differing in molecular weight between crosslinks $M_c$ ramp loaded with a Berkovich indenter to three maximum loads: 1 mN, 5 mN and 15 mN. The average $M_c$ is twice as high for E8 (black) than for E3 (gray).

### B. Nanoindentation contact creep with a spherical indenter

To determine whether it is possible to measure contact creep responses within the linear viscoelastic regime of polymer deformation, nanoindentation creep experiments were conducted with a spherical ruby indenter of $R = 500$ μm to the same five maximum loads as used in conical ramp indentation ($P_{max} = 1$, 5, 10, 15, and 30 mN) via ramp and step loading for the two epoxy samples, E3 and E8. Comparison of the load-displacement $P$–$h$ response with the Berkovich and spherical indenter geometries to the same $P_{max}$ (15 mN) illustrates the difference between the viscoelastic and the viscoelastoplastic regimes (Fig. 4). The percent of plastic or absorbed work, expressed as the ratio of final displacement at final unloading $h'_f$ to the maximum displacement $h_{max}$, was 39.4% for the Berkovich geometry and only 11.6% for the spherical geometry in E3. This confirms that the material response to the spherical indentations was predominantly viscoelastic under the loading rates considered. This conclusion is supported by the Tabor contact strain calculated for this spherical indenter geometry[26]

$$\epsilon = 0.2\,\frac{a}{R} \quad , \tag{8}$$

where $a$ is the radius of the contact area and $R$ is the radius of the spherical indenter. For the $P_{max}$ considered, the strains thus calculated ranged between 0.3% and 0.8%, indicating that the spherical indentations were well within the elastic limit for these polymers (typically between 1% and 2%[27]). Van Landingham et al. noted that creep compliance measurements on an epoxy (different from those considered herein) via a 10 μm radius conical tip appeared to be approaching linear viscoelastic behavior for the lowest loads applied in that study ($P_{max} = 0.2$ mN).[15] The corresponding strains in those experiments was ⩾4% and thus apparently exceeded the elastic limit of those materials under the conditions cited. Incidentally, for polymers with elastic strain limits near 1% and an instrumented indenter with load resolution on the order of 0.1 mN, a 500 μm radius is one of the smallest indenter radii that can be used while remaining within the elastic deformation regime. (This indenter radius induced contact strains of 0.8% at a maximum depth of 360 nm and load $P_o$ of 1 mN. For the polymers considered herein, indenters of smaller radii would require greater load resolution such that $P_o < 1$ mN to maintain contact strains $\epsilon < 1\%$). Although the strains induced by the two indenter geometries cannot be directly compared (the Berkovich induces strains ⩾1% at the cone apex), the average applied stresses may be estimated as the quotient of load to projected contact area ($\sigma_e$, akin to indentation hardness). Average stress imposed by the spherical indenter ranged from 5.5 to 18 MPa (depending on $P_{max}$), while the average stress imposed by the Berkovich indenter ranged from 194 to 470 MPa for the same range of $P_{max}$. Responses to these applied stress ranges are in agreement with published values of yielding; for example, amorphous polycarbonate has a yield strength of 62.1 MPa, which is well above stresses under the spherical indenter geometry but less than the lowest stress applied by the Berkovich indenter geometry.[28]

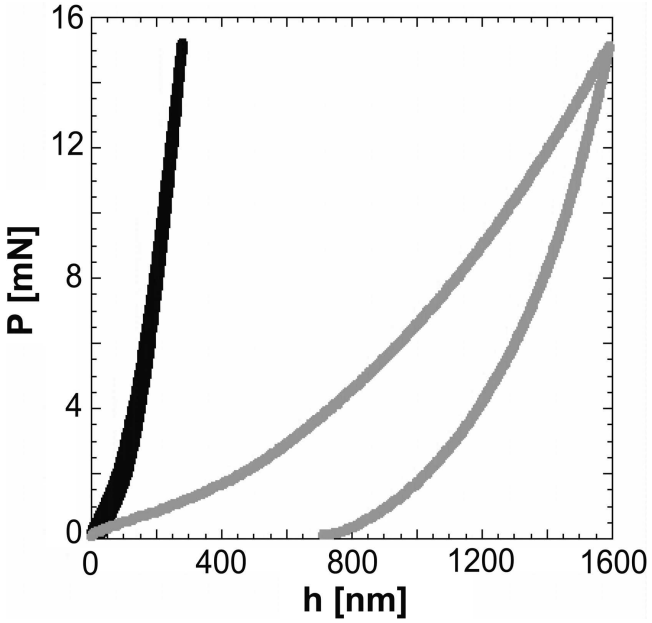


FIG. 4. Load-displacement response for epoxy (E3) ramp loaded to a maximum load of 15 mN for both a Berkovich indenter (gray) and a spherical indenter of radius $R = 500$ μm (black). Here, the creep segment at maximum load has been removed.

The low strains attainable with the large spherical indenter geometry enable contact creep experiments within the elastic strain limit of the material. As depicted in Fig. 5(a), contact creep via the spherical probe demonstrate $J_c(t)$ that is independent of both $P_{max}$ and d$P$/d$t$. Additionally, the magnitude of $J_c(t)$ is lower by an order of magnitude as compared with that obtained with a Berkovich indenter geometry for these polymers. Results reported by Van Landingham et al. display a similar trend over the same load range: a decrease in contact creep compliance obtained with a blunted conical indenter as compared with that obtained with a Berkovich indenter for the same polymers.[15] As expected, this decrease in $J_c(t)$ for the blunted cone was more subtle, as $\sigma_e$ differed by a factor of two, while in the current study, $\sigma_e$ differs by a factor of 10–20. In contrast with experiments that use a Berkovich or conical indenter geometry, for which error in $J_c(t)$ is significantly less than differences in $J_c(t)$ measured at different $P_{max}$ for a given polymer and loading rate, the error obtained on $J_c(t)$ measured with spherical indenter geometries indicates no statistically significant effect of load on $J_c(t)$. Of course, Fig. 5

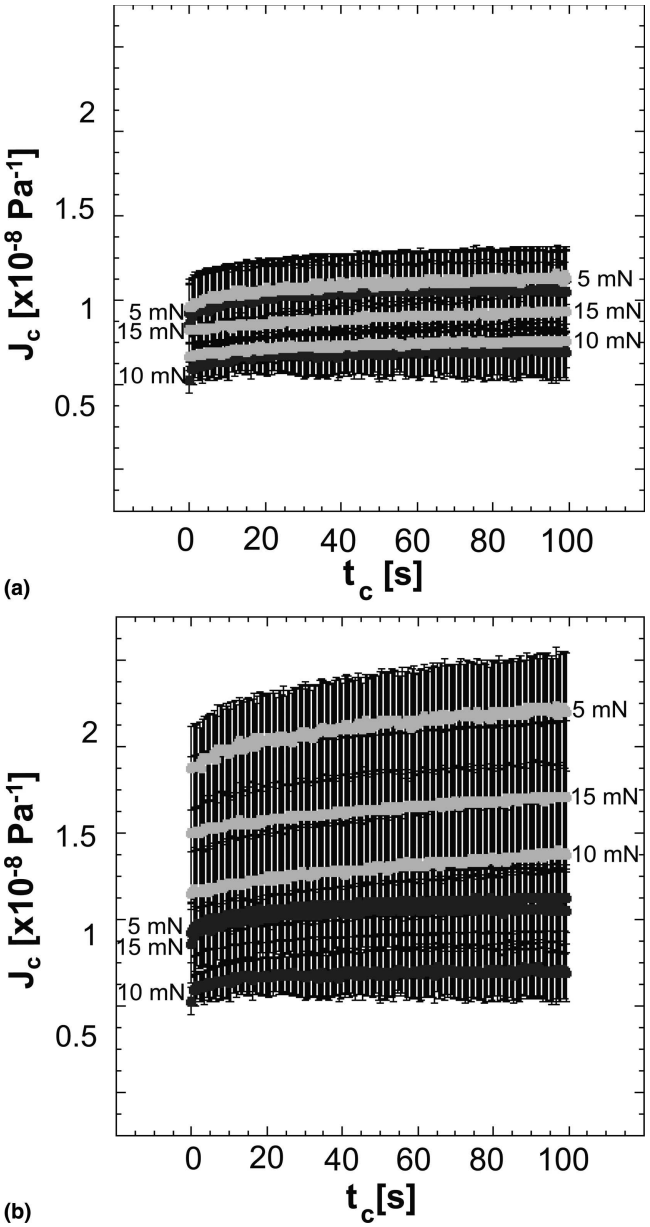


FIG. 5. (a) Comparison of creep compliance $J_c(t)$ for step (black) and ramp (gray) loading measured with a spherical indenter of radius $R = 500$ μm for a single epoxy (E3). $J_c(t)$ is not dependent on load or loading rate, as shown in the overlap between step and ramp loading for three maximum loads: 1, 5, and 15 mN. (b) Comparison of $J_c(t)$ for two epoxies differing in molecular weight between crosslinks $M_c$ under ramp loading with a spherical indenter of $R = 500$ μm to three maximum loads: 1, 5, and 15 mN. $M_c$ of E8 (black) is twice that of E3 (gray).

also demonstrates that the experimental scatter in $h(t)$ and thus in $J_c(t)$ is increased for spherical indenters of large $R$, in part because the change in load at the point of initial contact with the surface is less significant than that for a sharp indenter geometry. As noted, clear demonstration of the linear viscoelastic regime implies additivity; i.e., a given linear viscoelastic model fit to one set of data for a given material can accurately predict the creep response under varied loading times and maximum loads.[10]

### C. Structural and physical determinants of creep compliance

The interdependence of certain synthesis routes, structural characteristics, and physical-mechanical properties of polymers makes correlations of structure-property relations challenging, as demonstrated by the description of deformation states, including creep via spring-dashpot continuum models. However, certain subsets of the polymers considered herein enable consideration of structural determinants for $J_c(t)$ when linear viscoelastic deformation conditions are met, as well as speculation of microstructural determinants of creep and creep compliance rates when these conditions are not met.

Figure 2(b) illustrates creep compliance via Berkovich indentation for which the small strain assumptions of linear viscoelasticity are not met. Despite this quantitative limitation, $J_c(t = 10\ \text{s})$ of eight polymers at $P_{max} = 3$ and 15 mN correlates most strongly with monomer steric hindrance at a given load; it should be noted that molecular weight among these polymers also differs. Polyethylene is expected to exhibit the greatest molecular chain mobility per unit length, due to the extremely simple monomer structure of this polymer, as shown in Table I, and this correlates with the fact that PE exhibits the greatest $J_c(t)$ at all conditions. Polypropylene (PP) also has a very simple monomer structure and was the fourth most creep compliant polymer tested. Both the PE and PP samples were semicrystalline and tested above their glass transition temperatures. Although it is expected that the amorphous regions of these materials would still creep readily, this microstructural heterogeneity resulted in rather complex behavior. For example, while PP shows a slight increase in $J_c(t)$ with $P_{max}$, PE is the only polymer to exhibit a decrease in $J_c(t)$ with increasing $P_{max}$.

Contact creep response of the six amorphous polymers indicates the relative importance of monomer steric hindrance and molecular weight. The polycarbonate (PC) backbone contains two benzene rings and has significantly reduced chain mobility due to this rigidity. Consequently, amorphous PC exhibits lower $J_c(t)$ than that of PE or PP, despite the extremely low $M_w$ of PC. This indicates that steric hindrance is more important than $M_w$ in determining the magnitude of contract creep compliance $J_c(t)$ for a given applied contact load $P_{max}$. However, molecular weight does have a modest effect on $J_c(t)$, as demonstrated by the comparison of the two poly(methyl methacrylates) considered, PL and LU. The $M_w$ of PL is more than twice that of LU, but otherwise these amorphous polymers are identical; this difference in $M_w$

correlates with an 8% decrease in $J_c(t)$ for PL with respect to LU. In addition, the two epoxies have different molecular weight between crosslinks or entanglement points quantified as $M_c$, which has a corresponding effect on $J_c(t)$: E3 ($M_c$ = 380 g/mol) exhibited a $J_c(t)$ significantly lower at all loads considered than that of E8 ($M_c$ = 818 g/mol) due to the relatively lower chain mobility of epoxy E3.

The microstructural dependency of $J_c(t)$ is underscored by the rankings of the six glassy network polymers depicted in Fig. 6(a) considered at the same $P_{max}$. While $J_c(t = 0)$ simply reflects the relative stiffness of these polymers during the loading phase, the rates of change in the (steady-state) contact creep compliance do not follow this same trend. Figure 6(b) shows this contact creep compliance rate over a 60 s dwell for polymers listed in order of increasing $M_w$. Figure 6 illustrates two important points. First, the (steady-state or $t > 5$ s) rate of creep compliance is unique to each polymer, as demonstrated by distinct $d\{log[J_c(t)]\}/d[log(t)]$ in Fig. 6(b). Second, unlike material responses during the loading phase, which correlate positively with steric hindrance to chain mobility, the primary factor in the rate of creep compliance (and, by definition, the rate of change of contact area) is the $M_w$ or entanglement distance of the polymers.

The most striking illustration of this point is the comparison of the two PMMA samples, PL and LU. Although PL and LU have the same monomer structure and $T_g$, the $M_w$ of PL is nearly 2.5 times greater than that of LU. The local steric hindrance of a given polymer segment is equivalent, so these polymers would be expected to deform to approximately the same depth $h$ for a given load $P$. By extension, the magnitude of $J_c(t = 0)$ would be expected to be quite similar, and this is what is observed experimentally [Fig. 6(a)]. However, these polymers of differing $M_w$ show dramatic differences in the creep compliance rate, with the PMMA of greater $M_w$ demonstrating the higher rate of contact creep compliance. Another clear example of the apparent effect of $M_w$ on contact creep compliance rate is demonstrated by PC; the fourth stiffest polymer tested, PC exhibits the lowest creep compliance rate. We hypothesize that this is due to the low $M_w$ of PC, which signifies very little structural continuity/connectivity between the deformed and undeformed regions of material. As shown schematically in Fig. 7, when contact stress is applied to a material comprising many short macromolecules, such as PC, the deformation is likely to translate entire chains to new locations without requiring storage of large internal strains within molecules that bridge deformed and undeformed regions in the material. In contrast, when contact stress is applied to a material composed of long macromolecules, it is likely that a single polymer chain may reside both in surface regions of high strain (near the indenter) and low

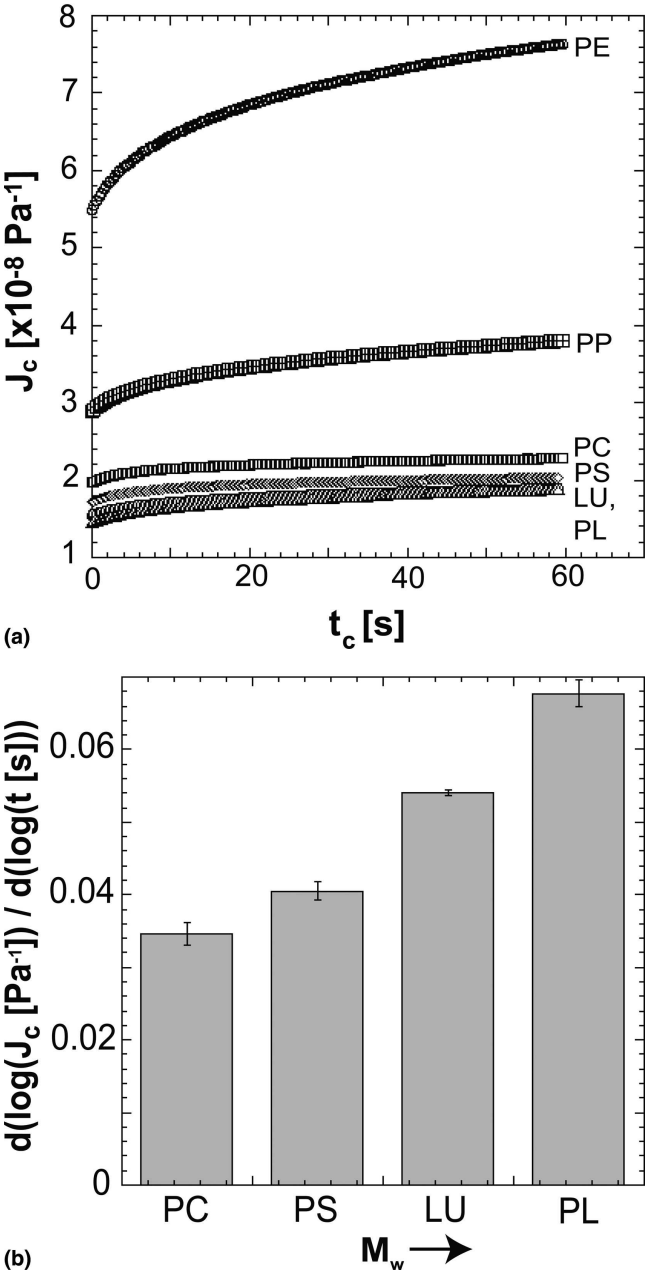


FIG. 6. (a) Contact creep compliance $J_c(t)$ under ramp loading (0.5 mN/s) to 30 mN via Berkovich (sharp) probe for six polymers as a function of $t_c$. (b) Rate of creep compliance $dJ_c(t)/dt$ increases with molecular weight $M_w$ for the amorphous polymers tested in (a): PC, PS, LU, and PL. Though monomer structure and physical properties also differ among these polymers, LU and PL differ principally in $M_w$.

or zero strain (far from the indenter). In fact, the contact radii $a$ ranged from 0.8 to 4.8 μm for contact creep experiments on the amorphous polymers considered herein, while the contour lengths $L$ of the amorphous polymers of highest and lowest $M_w$ were 0.7 μm (PS) and 7.3 μm (PMMA), respectively. (Contour length $L$[29] was estimated as the product of the number of segments $n$ and monomer length $l$, given published radii of gyration for PS[30] and PMMA.[31]) While increased $M_w$ causes

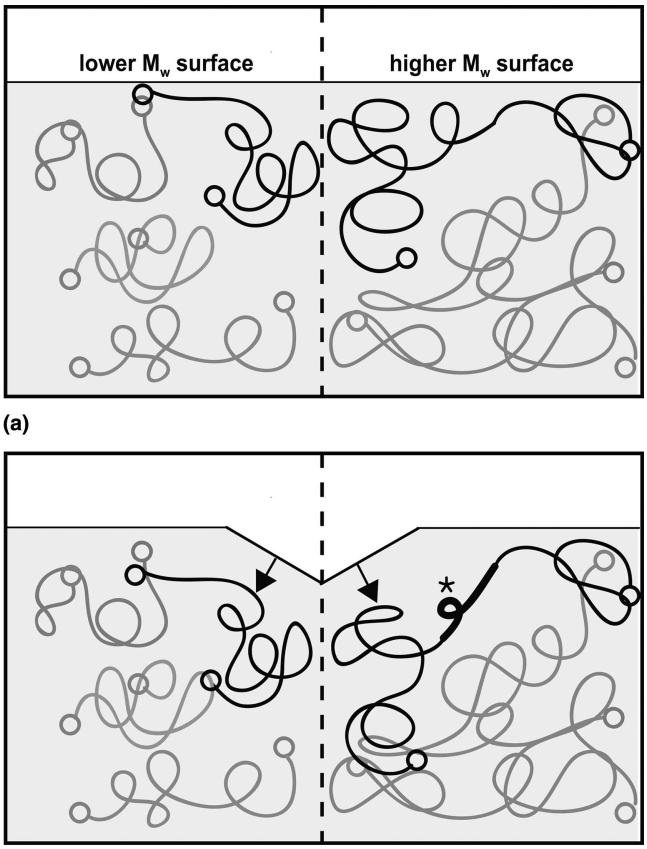


FIG. 7. Schematic illustrations of high (left) and low (right) molecular weight polymer samples (a) before and (b) after loading via a sharp indenter. Actual contact radii $a$ ranged from 0.8 to 4.8 μm, while contour lengths $L$ of the amorphous polymers of highest and lowest $M_w$ were 0.7 μm (PS) and 7.3 μm (PMMA), respectively. The asterisk (*) in (b) indicates a region of high intramolecular tension, which causes continued molecular displacement to reduce the internal strain.

a modest increase in stiffness during the loading phase, this structural connectivity between highly strained and unstrained material regions has a more dominant effect during contact creep. Under constant applied load, as during indentation creep, it is hypothesized that a long-chained or high $M_w$ material will decrease the intramolecular tension induced by the applied creep load by either displacing the portion of the molecule under low strain toward the highly strained region of the contact zone or by displacing the highly strained region of the molecule toward the "anchored" region of low strain. In either scenario, the connectivity decreases the resistance of the material to further indenter penetration and results in a faster rate of change in the creep compliance. In the case of the short-chained polymer, such a driving force to reduce intramolecular strain would be decreased by the lack of long-range molecular continuity/connectivity between the highly strained and unstrained material regions.

Although there is no clear dependence of $J_c(t)$ on $P_{max}$ or $dP/dt$ for these polymers evaluated with a sphere of $R = 500$ μm, there remains a clear effect of polymer structure on $J_c(t)$ within the linear viscoelastic deformation regime. Figure 5(b) compares $J_c(t)$ for expoxies E3 and E8 to $P_{max} = 5$, 10, and 15 mN under ramp loading. Although there is no direct dependence on $P_{max}$, almost all $J_c(t)$ measured for the polymer of greater $M_c$ and thus higher chain mobility (E8) exceeded those of the lower $M_c$ polymer (E3). This result indicates that the contact creep response of a polymer, measured in the linear viscoelastic regime, will reflect changes in polymer structure while remaining independent of loading conditions.

## V. CONCLUSIONS

Contact creep compliance is a useful metric that quantifies a unique mechanical response of time-dependent materials. The analysis of contact creep compliance experiments to quantify the mechanical response of polymers is conceptually straightforward but includes several important experimental and analytical caveats. Herein, we have detailed the evolution and assumptions of the contact creep compliance analysis in the context of linear viscoelastic deformation and have experimentally determined the conditions under which such analysis may be reasonably applied by identifying contact strains for which $J_c(t)$ is not a function of creep load. In addition, we have considered the extent to which the molecular description of amorphous polymers defines the extent and rate of contact creep compliance.

There are two main conclusions to be drawn from these findings. First, nanoscale contact creep experiments conducted with sharp and/or conical indenter geometries on polymeric surfaces cannot be interpreted accurately through recourse to current linear viscoelastic analyses of contact. However, linear viscoelastic responses may be obtained via a spherical indenter geometry of sufficiently large $R$ that induce maximum strains less than the elastic strain limit. This limitation should be considered for contact creep analysis of thin films, for which finite thickness also requires small indentation depths. We note that linear viscoelastic solutions can be applied to indentation creep analysis under large strains, such as in conical indentation, provided that the nonlinear and plastic deformations can be analytically decoupled from the total creep response. Second, although monomer steric hindrance correlates strongly with polymer stiffness [and the initial magnitude of the contact creep compliance $J_c(t = 0)$], molecular weight or molecular weight between crosslinks correlates strongly with contact creep compliance rate.

## ACKNOWLEDGMENTS

The authors gratefully acknowledge support from the DuPont–Massachusetts Institute of Technology Alliance,

as well as helpful discussion and material samples from Dr. Greg Blackman of DuPont Central Research & Development. We also thank Dr. Mark Van Landingham and Dr. Thomas Juliano for providing and discussing experimental data and interpretation and for providing epoxy samples as reported in Lesser et al.[20] Finally, we thank Dr. James Smith and Dr. Stephen Goodes of Micro Materials, Ltd. for insightful technical discussion and assistance. C.A.T. acknowledges support though the National Defense Science and Engineering Graduate Fellowship program.

## REFERENCES

1. W.C. Oliver and G.M. Pharr: An improved technique for determining hardness and elastic-modulus using load and displacement sensing indentation experiments. *J. Mater. Res.* **7,** 1564 (1992).
2. S.A.S. Asif, K.J. Wahl, R.J. Colton, and O.L. Warren: Quantitative imaging of nanoscale mechanical properties using hybrid nanoindentation and force modulation. *J. Appl. Phys.* **90,** 1192 (2001).
3. J.L. Loubet, W.C. Oliver, and B.N. Lucas: Measurement of the loss tangent of low-density polyethylene with a nanoindentation technique. *J. Mater. Res.* **15,** 1195 (2000).
4. A.H.W. Ngan and B. Tang: Viscoelastic effects during unloading in depth-sensing indentation. *J. Mater. Res.* **17,** 2604 (2002).
5. H. Lu, B. Wang, J. Ma, G. Huang, and H. Viswanathan: Measurement of creep compliance of solid polymers by nanoindentation. *Mech. Time-Depend. Mater.* **7,** 189 (2003).
6. A.C. Fischer-Cripps: A simple phenomenological approach to nanoindentation creep. *Mater. Sci. Eng. A* **385,** 74 (2004).
7. M.R. VanLandingham, P.L. Drzal, and C.C. White: Indentation creep and relaxation measurements of polymers, in *Fundamentals of Nanoindentation and Nanotribology III,* edited by K.J. Wahl, N. Huber, A.B. Mann, D.F. Bahr, and Y-T. Cheng (Mater. Res. Soc. Symp. Proc. **841,** Warrendale, PA, 2005), R5.5.
8. H. Lu, G. Huang, B. Wang, A. Mamedov, and S. Gupta: Measurements of viscoelastic properties of SWNT/polymer composite films using nanoindentation, in *Fundamentals of Nanoindentation and Nanotribology III,* edited by K.J. Wahl, N. Huber, A.B. Mann, D.F. Bahr, and Y-T. Cheng (Mater. Res. Soc. Symp. Proc. **841,** Warrendale, PA, 2005), R4.5.
9. S. Yang, Y.W. Zhang, and K.Y. Zeng: Analysis of nanoindentation creep for polymeric materials. *J. Appl. Phys.* **95,** 3655 (2004).
10. M.L. Oyen: Spherical indentation creep following ramp loading. *J. Mater. Res.* **20,** 2094 (2005).
11. C.A. Tweedie and K.J. Van Vliet: Nanomechanical quantification of energy absorption, in *Fundamentals of Nanoindentation and Nanotribology III,* edited by K.J. Wahl, N. Huber, A.B. Mann, D.F. Bahr, and Y-T. Cheng (Mater. Res. Soc. Symp. Proc. **841,** Warrendale, PA, 2005), R5.6.
12. T.C.T. Ting: The contact stresses between a rigid indentor and a viscoelastic half-space. *J. Appl. Mech.* **88,** 845 (1966).
13. E.H. Lee and J.R.M. Radok: The contact problem for viscoelastic bodies. *J. Appl. Mech.* **27,** 438 (1960).
14. L. Cheng, X. Xia, L.E. Scriven, and W.W. Gerberich: Spherical-tip indentation of viscoelastic material. *Mech. Mater.* **37,** 213 (2005).
15. M.R. VanLandingham, N-K. Chang, P.L. Drzal, C.C. White, and S-H. Chang: Viscoelastic characterization of polymers using instrumented indentation—I. Quasi-static testing. *J. Polym. Sci. B: Polym. Phys.* **43,** 1794 (2005).
16. Y-T. Cheng and C-M. Cheng: Modeling indentation in linear viscoelastic solids, in *Fundamentals of Nanoindentation and Nanotribology III,* edited by K.J. Wahl, N. Huber, A.B. Mann, D.F. Bahr, and Y-T. Cheng (Mater. Res. Soc. Symp. Proc. **841,** Warrendale, PA, 2005), R11.2.
17. B.J. Briscoe, L. Fiori, and E. Pelillo: Nano-indentation of polymeric surfaces. *J. Phys. D* **31,** 2395 (1998).
18. M. Vandamme and F. Ulm: Viscoelastic solutions for conical indentation. (2005, unpublished).
19. I.N. Sneddon: The relation between load and penetration in the axisymmetric boussinesq problem for a punch of arbitrary profile. *Int. J. Eng. Sci.* **3,** 47 (1965).
20. A.J. Lesser and K.J. Calzia: Molecular parameters governing the yield response of epoxy-based glassy networks. *J. Polym. Sci. B: Polym. Phys.* **42,** 2050 (2004).
21. L.S. Loo, R.E. Cohen, and K.K. Gleason: Chain mobility in the amorphous region of nylon 6 observed under active uniaxial deformation. *Science* **288,** 116 (2000).
22. S. Shimizu, T. Yanagimoto, and M. Sakai: The pyramidal indentation load-depth curve of viscoelastic materials. *J. Mater. Res.* **14,** 4075 (1999).
23. M. Sakai: Indentation rheometry for glass-forming materials: *J. Non-Cryst. Solids* **282,** 236 (2001).
24. Y-T. Cheng and C-M. Cheng: Relationships between initial unloading slope, contact depth, and mechanical properties for conical indentation in linear viscoelastic solids. *J. Mater. Res.* **20,** 1046 (2005).
25. C.A. Tweedie and K.J. Van Vliet: On the volumetric recovery and fleeting hardness of time-dependent materials (polymers). (2006, unpublished).
26. D. Tabor: *The Hardness of Metals* (Clarendon, London, UK, 1951).
27. J.D. Ferry: *Viscoelastic Properties of Polymers,* 3rd ed. (John Wiley & Sons, New York, 1980).
28. R.F. Brady: *Comprehensive Desk Reference of Polymer Characterization and Analysis* (Oxford University Press, Washington, DC, 2003).
29. R.J. Young and P.A. Lovell: *Introduction to Polymers,* 2nd ed. (Chapman & Hall, New York, 1991).
30. F. Dinelli, G.J. Leggett, and P.H. Shipway: Nanowear of polystyrene surfaces: Molecular entanglement and bundle formation. *Nanotech.* **16,** 675 (2005).
31. R.D. Priestly, C.J. Ellison, L.J. Broadbelt, and J.M. Torkelson: Structural relaxation of polymer glasses at surfaces, interfaces, and in between. *Science* **309,** 456 (2005).
32. E.H. Lee: Stress analysis in visco-elastic bodies. *Quart. Appl. Math.* **13,** 183 (1955).
33. H.R. Hertz: *On the Contact of Two Elastic Solids* (MacMillan, 1882).
34. See Eq. 25c of Ref. 12.

## APPENDIX A: GENERAL FRAMEWORK OF EXISTING SOLUTIONS FOR $J(t)$

Lee and Radok first recognized the difficulty in obtaining a solution to calculate the stress distribution for Hertzian (elastic, spherical) contact between a rigid indenter and a viscoelastic body. This complication arises because conventional approaches to linear viscoelastic deformation had applied the Laplace transform (i.e., solving for linear operators) to map this time-dependent solution to the corresponding elastic solution.[32] Although this approach could be used to determine, for example,

the viscoelastic solution to creep of a viscoelastic material under a uniform uniaxial stress [Fig. 1(a)], the Laplace transform is not necessarily valid when both the boundary position and boundary conditions change with time, as is characteristic of spherical or conical contact for increasing/decreasing displacement, because neither the stress nor the strain can be uniquely determined at each deformation time point and thereafter transformed to time-space.

Lee and Radok proposed to instead adopt a single elastic solution for the boundary conditions of the actual viscoelastic problem and then substitute elastic constants with viscoelastic operators. They verified this approach for the specific problem of spherical elastic contact loading, i.e., increasing contact area as would be expected during loading or creep. As Ting's more general analysis—the linear viscoelastic analogue to the solutions of Sneddon[19]—extends this approach to other indenter geometries and loading conditions, it is necessary to outline the assumptions common to both solutions, hereafter referred to as the LR- or T-solution. Both the LR- and T-solutions assume linear viscoelasticity in that the functions that define the constitutive relation of the viscoelastic material are linear operators:

$$As_{ij} = Be_{ij} \quad , \tag{A1}$$

$$A'\sigma_{ii} = B'\epsilon_{ii} \quad , \tag{A2}$$

where $s_{ij}$ and $e_{ij}$ are the deviatoric stress and strain components, respectively, and $\sigma_{ij}$ and $\epsilon_{ij}$ are the total stress and strain, respectively. This restriction enables mapping of a linear elastic solution or inversion of integral forms of such solutions, where the shear elastic modulus $G$ is exactly equal to $B/2A$ for an incompressible material (i.e., $\nu = 1/2$) and implies several characteristics of material behavior and of $J(t)$ as a function of loading conditions. LR then adopts the solution of Hertz[33] for a contact pressure distribution that varies not only with radial distance from the central loading axis $r$ but also with time $t$:

$$p(r,t) = \frac{4Q}{\pi R} f(r) \quad , \tag{A3}$$

where $f(r)$ is the indenter shape function relating $h(r, a)$ (see Appendix B) and $a(t)$ is the contact radius at the free surface of the indented material. The assumption of $\nu = 1/2$ is assumed by LR for simplicity but is not required of the solution. The LR-solution determines $J(t)$ based on the deviatoric strain $e_{ij}$. The two key equations of the LR-solution are the inverse transform to real time of the total indentation force $P$:

$$A[P(t)] = \frac{8B[Rh(t)]^{3/2}}{3R} \quad , \tag{A4}$$

where $A$ and $B$ are the linear viscoelastic operators, $R$ is the spherical indenter radius, and the creep compliance in shear is determined as a function of the transform of deviatoric strain $e_{ij}$ in terms of the transform variable $s$:

$$\overline{A} = \frac{1}{2} J(s)s, \; \overline{B} = 1 \quad . \tag{A5}$$

For any given $P(t)$ such that $a(t)$ is increasing, $J(t)$ can then be determined as

$$\int_0^t \frac{1}{2} J(t-\tau) \frac{\mathrm{d}P}{\mathrm{d}\tau} \mathrm{d}\tau = \frac{8}{3} \sqrt{R}[h(t)]^{3/2} \quad . \tag{A6}$$

In contrast, the T-solution maintains and inverts the integral form of $p(r, t)$ in terms of elastic indentation depth $h(t)$. As a result, this is a more general viscoelastic solution of contact pressure distribution that can be expressed for any loading history [$a(t)$ increasing or decreasing]and indenter geometry; Ting explicitly demonstrates that the pressure distribution solution of Lee and Radok[13] is recovered for identical conditions. The two key equations of the T-solution are the relation between surface displacement along the loading axis $u(z = 0)$ and the first of two linear viscoelastic operators Ting calls $\phi(t)$:

$$u(r, 0, t) = \int_{0-}^{t} \phi(t-s) \frac{\partial}{\partial s} \int^{a(t)0} \beta(r,x) x p(x,s) \mathrm{d}s \mathrm{d}\tau \quad , \tag{A7}$$

where $\beta$ is a Bessel function of the first kind [typically denoted by $J$ but modified here to avoid confusion with $J(t)$] and $r$ is radial distance along the free surface. The elastic solution to Eq. (A7) is

$$\begin{aligned} u_e(r,0,t) &= h(t) - f(r)H(t) \\ &= \frac{1-\nu}{G} \int_{0-}^{a(t)} \beta(r,x) x p_e(x,t) \mathrm{d}x \quad , \end{aligned} \tag{A8}$$

where $f(r)$ is the indenter shape function relating $h(r, a)$ (see Appendix A), and $H(t)$ is the Heaviside step function defining the edge of the contact zone. By separating any loading history into integrals of the form of Eq. (A8), the solution for the actual pressure distribution $p(r, t)$ can be determined as a function of the elastic solution and $\psi(l)$, the second of Ting's linear viscoelastic operators. Ting notes that for constant Poisson's ratio $\nu$, $\psi(t)$ has the form of the relaxation modulus in shear $G(t)$:

$$p(r,t) = f\left[\frac{1-\nu}{G} p_e(r,t) \psi(t)\right] \quad . \tag{A9}$$

and $\phi(t) = 1/\psi(t)$ has the form of creep compliance in shear $J(t)$. Ting states that for a monotonic increase in

contact radius $a(t)$, $\phi(t)$ can be related to the elastic expression of total pressure $(1 - \nu)P_e(t)/G$ as

$$\frac{(1-\nu)P_e(t)}{G} = P(0)\phi(t)H(t) \quad , \tag{A10}$$

where $G$ is the shear elastic modulus. Then, for a constant and instantaneously applied load $P(0) = P_o$, the left hand side of Eq. (A10) can be expressed as an integral of the shape function $f(r)$,[34] such that $\phi(t)$ can be determined generally as

$$\phi(t) = \frac{4\int_0^{a(t)} \frac{r^2}{\sqrt{a^2(t) - r^2}} \frac{d}{dr} f(r) dr}{P_o H(t)} \quad . \tag{A11}$$

For this constant load and changing contact area, $\phi(t)$ does not identically (or necessarily) represent $J(t)$, which assumes a constant applied stress $\sigma_o$ but rather the history of this contact area evolution. In fact, $\sigma(t) = (1 - \nu)J(t)$ for constant $\nu$ [see Eqs. (2) and (3)]. Here, we denote this as contact creep compliance $J_c(t)$. As creep compliance implies deformation in the linear (visco)elastic regime and we discuss deviation from this response for a range of indentation-enabled measurements of creep compliance, $J_c(t)$ is more generally an apparent creep compliance.

## APPENDIX B: INDENTER SHAPE FUNCTIONS AND *h*(*a*)

As stated by Ting, the displacement along the loading axis $u_z$ can be expressed as:

$$u_z = h(t) - f(r)H(t) \quad , \tag{A12}$$

where $f(r)$ is an indenter shape (or geometric) function that relates the depth of indentation $h(t)$ to $a(t)$ under the condition that Eq. (A12) is zero at $r = a(t)$. [Note that $h(t)$ is actually the contact depth of indentation, typically denoted as $h_c(t)$.] As a result, the relationship between $h(t)$ and $a(t)$ includes but not is identical to $f(r)$. For example, for a spherical indenter of radius $R$,

$$f(r) = R - \sqrt{R^2 - r^2} \tag{A13}$$

and reduces to $f(r) = r^2/2R$ for $r \ll R$ as is typically assumed for "small strain" applications, such that

$$h(t) = \frac{[a(t)]^2}{R} \quad , \tag{A14}$$

and thus there is a difference of a factor of 2 between $f(r)$ and $h(t)$ in this particular case. This point must be considered when applying solutions expressed in terms of $a(t)$ which must be calculated from instrumented indentation data as a function of $h(t)$, which is measured experimentally.